

Relativistic Calculation Of $K\beta$ Hypersatellite Energies and Transition Probabilities for Selected Atoms with $13 \leq Z \leq 80$

A. M. Costa^{†§‡}, M. C. Martins^{†§}, J. P. Santos^{‡§}, P. Indelicato^{||} and F. Parente^{‡§}

[†] Departamento de Física, Faculdade de Ciências, Universidade de Lisboa, Campo Grande, 1749-016 Lisboa, Portugal

[‡] Departamento de Física, Faculdade de Ciências e Tecnologia, Universidade Nova de Lisboa, Monte de Caparica, 2825-114 Caparica, Portugal

[§] Centro de Física Atómica da Universidade de Lisboa, Av. Prof. Gama Pinto 2, 1649-003 Lisboa, Portugal

^{||} Laboratoire Kastler Brossel, École Normale Supérieure; CNRS; Université P. et M. Curie - Paris 6, Case 74; 4, place Jussieu, 75252 Paris CEDEX 05, France

Abstract. Energies and transition probabilities of $K\beta$ hypersatellite lines are computed using the Dirac-Fock model for several values of Z throughout the periodic table. The influence of the Breit interaction on the energy shifts from the corresponding diagram lines and on the $K\beta_1^h/K\beta_3^h$ intensity ratio is evaluated. The widths of the double-K hole levels are calculated for Al and Sc. The results are compared to experiment and to other theoretical calculations.

PACS numbers: 31.25.Jf, 32.30Rj, 32.70.Cs

29 December 2021

[‡] To whom correspondence should be addressed (amcosta@fc.ul.pt)

1. Introduction

Energies and transition probabilities of $K\beta$ hypersatellite lines are evaluated in this work for selected atoms throughout the periodic table. In a previous paper [1], we reported on calculated values of $K\alpha$ hypersatellite line energies for atoms with $12 \leq Z \leq 30$.

A hypersatellite line is an X-ray line for which the initial state has two vacancies in the same shell. This is the case, for example, when a double ionized K-shell state decays through the transition of one M-shell electron. Lines corresponding to $1s^{-2} \rightarrow 1s^{-1}3p^{-1}$ transitions, where $n\ell^{-k}$ means k vacancies in the $n\ell$ subshell, are called $K\beta_{1,3}^h$ hypersatellite lines.

Atoms where a whole inner shell is empty while the outer shells are occupied were first named hollow atoms by Briand *et al* [2] and are of great importance for studies of ultrafast dynamics in atoms far from equilibrium and with possible wide-ranging applications in physics, chemistry, biology, and materials science [3].

Very scarce experimental data exist on energies of K hypersatellite lines, due to the low probability of creation of the initial two K holes. Briand *et al* [4] used a coincidence method to study the K hypersatellite spectrum in Ga and measured a 390 eV energy shift for the $K\beta^h$ lines relative to the corresponding diagram lines. Energies of $K\beta^h$ hypersatellite lines were later measured by Briand *et al* [5, 6] for Mn, Ga and In. Diamant *et al* [7] obtained high resolution $K\beta_{1,3}^h$ and $K\alpha^h$ hypersatellite spectra of Fe, using monochromatized synchrotron radiation photoexcitation. Similar work has been performed for Cr $K\beta^h$ hypersatellite spectra [8]. More recently, this work has been extended to Ti [9].

On the theoretical side, calculations of the energies and transition probabilities of $K\beta_{1,3}^h$ hypersatellite lines have been performed [10] using a Dirac-Hartree-Slater approach. This approach employs a local approximation to the atomic potential. With the wave functions obtained from this potential, perturbation calculations were then used to obtain the energies. Diamant *et al* [7] performed relativistic multi-configuration Dirac-Fock calculations for the $K\beta_{1,3}^h$ hypersatellite lines of Fe to compare with their own experimental findings.

The energy shifts between the $K\beta_{1,3}^h$ hypersatellite lines and the corresponding $K\beta_{1,3}$ diagram lines (as the $K\alpha^h$ - $K\alpha$ ones) are considered to be very sensitive to the Breit interaction. Chen *et al* [10] calculated the influence of the Breit interaction on these shifts, using a mathematical form appropriate for the local approximation employed. To check the importance of the Breit interaction, values of these shifts as well of the $K\beta_1^h/K\beta_3^h$ intensity ratios were calculated in this work for selected values of Z , with and without inclusion of the this interaction.

Using the results of our calculations, we were able to obtain the widths of the $1s^{-2}$ two-hole levels of Al and Sc.

2. Calculation of atomic wave functions and energies

Bound state wave functions and radiative transition probabilities were calculated using the multi-configuration Dirac-Fock program of J. P. Desclaux and P. Indelicato [11, 12, 13]. The program was used in single-configuration mode because correlation was found to be unimportant for the energies and probabilities transition. The wave functions of the initial and final states were computed independently, that is, atomic orbitals were fully relaxed in the calculation of the wave function for each state, and non-orthogonality was taken in account in transition probability calculations.

In order to obtain a correct relationship between many-body methods and quantum electrodynamics (QED) [14, 15, 16, 17], one should start from the no-pair Hamiltonian

$$\mathcal{H}^{\text{no pair}} = \sum_{i=1}^N \mathcal{H}_D(r_i) + \sum_{i<j} \mathcal{V}(r_{ij}), \quad (1)$$

where $r_{ij} = |\mathbf{r}_i - \mathbf{r}_j|$, and \mathcal{H}_D is the one electron Dirac operator and \mathcal{V} is an operator representing the electron-electron interaction of order one in α , properly set up between projection operators $\Lambda_{ij}^{++} = \Lambda_i^+ \Lambda_j^+$ to avoid coupling positive and negative energy states

$$\mathcal{V}(r_{ij}) = \Lambda_{ij}^{++} V(r_{ij}) \Lambda_{ij}^{++}. \quad (2)$$

In nonrelativistic quantum mechanics the interaction between charged particles is described by an operator associated to the potential energy of interaction, $V(r_{ij})$, which is only a function of the distance between particles, r_{ij} . However, in quantum electrodynamics there exists no potential energy of interaction that depends on the coordinates of the interacting charged particles taken at the same time, since the charges interact not directly, but via the electromagnetic field. The operator for the interaction potential energy is replaced, in the first approximation, by the scattering matrix [18]

$$\mathcal{S}_{AB \rightarrow CD}^{(2)} = e^2 \int \bar{\psi}_D(y) \gamma_\mu \psi_B(y) D^c(y-x) \bar{\psi}_C(y) \gamma_\mu \psi_A(y) d^4y d^4x, \quad (3)$$

After performing the time integration of (3), one finds the following well known interaction potential, in Coulomb gauge and in atomic units,

$$g(r_{ij}) = \frac{1}{r_{ij}} \quad (4a)$$

$$- \frac{\boldsymbol{\alpha}_i \cdot \boldsymbol{\alpha}_j}{r_{ij}} \quad (4b)$$

$$- \frac{\boldsymbol{\alpha}_i \cdot \boldsymbol{\alpha}_j}{r_{ij}} \left[\cos\left(\frac{\omega_{ij} r_{ij}}{c}\right) - 1 \right] + (\boldsymbol{\alpha}_i \cdot \nabla_i)(\boldsymbol{\alpha}_j \cdot \nabla_j) \frac{\cos\left(\frac{\omega_{ij} r_{ij}}{c}\right) - 1}{\omega_{ij}^2 r_{ij}}, \quad (4c)$$

where ω_{ij} is the energy of the photon exchanged between the two electrons, $\boldsymbol{\alpha}_i$ are the Dirac matrices and $c = 1/\alpha$ is the speed of light. The first term (4a) represents the Coulomb interaction, the second one (4b) is the Gaunt interaction (magnetic interaction), and the last two terms (4c) stand for the retardation operator. In this

expression the ∇ operators act only on r_{ij} and not on the following wave functions. By a series expansion of the terms Eqs. (4b)-(4c) in powers of $\omega_{ij}r_{ij}/c \ll 1$ one obtains the Breit interaction, which includes the leading retardation contribution of order $1/c^2$. The Breit interaction is the sum of the Gaunt interaction (4b) and of the Breit retardation

$$g^B(r_{ij}) = \frac{\boldsymbol{\alpha}_i \cdot \boldsymbol{\alpha}_j}{2r_{ij}} - \frac{(\boldsymbol{\alpha}_i \cdot \mathbf{r}_{ij})(\boldsymbol{\alpha}_j \cdot \mathbf{r}_{ij})}{2r_{ij}^3}. \quad (5)$$

In the present calculation the electron-electron interaction is described by the sum of the Coulomb and the Breit interaction. Higher orders in $1/c$, coming from the difference between Eqs. (4c) and (5) are treated here only as a first order perturbation.

We use the Coulomb gauge as it has been demonstrated that it provides energies free from spurious contributions at the ladder approximation level and must be used in many-body atomic structure calculations [19].

Finally, from a full QED treatment, one also obtains the radiative corrections (important for the innermost shells) to the electron-nucleus interaction (self-energy and vacuum polarization). The one-electron self-energy is evaluated using the one-electron values of Mohr and coworkers [20, 21, 22]. The self-energy screening is treated with the Welton method developed in Refs. [23, 24, 25, 26]. This method yields results in close agreement (better than 5%) with *ab initio* methods based on QED [27, 28, 29, 30], without the huge amount of effort involved.

The vacuum polarization is evaluated as described in Ref. [31]. The Uehling contribution is evaluated to all orders by being included in the self-consistent field (SCF). The Wichmann and Kroll, and Källén and Sabry contributions are included perturbatively. These three contributions are evaluated using the numerical procedure from Refs. [32, 33].

3. Results

3.1. Introduction

We calculated the energy shifts of the $K\beta_{13}^h$ hypersatellite lines relative to the corresponding diagram lines for several atoms with $13 \leq Z \leq 80$, and the $K\beta_1^h$ and $K\beta_3^h$ energy shifts, and their relative intensities, for selected atoms with $18 \leq Z \leq 80$. The wave functions of the initial and final states were computed independently, that is, atomic orbitals were fully relaxed in the calculation of the wave function for each state.

In what concerns the precise identification of the $K\beta_{1,3}^h$ hypersatellite lines some comments are in order.

Depending on the configurations of the initial and final states, for the different values of Z , the number of transition lines that must be computed may range from only two, when the initial state has only closed shells, to several thousand, when unfilled shells exist.

For elements with filled shells, namely Ar, Ca, Zn, Kr, Sr, Pd, Cd, Xe, Ba and Hg the $1s^{-2}$ ground configuration corresponds to only one level, the 1S_0 level, and each of

the $K\beta^h$ lines is identified by a precise level transition,

$$\begin{aligned} K\beta_3^h: & \quad 1s^{-2} {}^1S_0 \rightarrow 1s^{-1}3p^{-1} {}^1P_1 \\ K\beta_1^h: & \quad 1s^{-2} {}^1S_0 \rightarrow 1s^{-1}3p^{-1} {}^3P_1. \end{aligned}$$

By analogy with the corresponding diagram lines, the line that corresponds to the larger transition energy value is labeled $K\beta_1^h$ and the other one is labeled $K\beta_3^h$.

For $Z \geq 29$ there are two sets of transition lines, separated in energy by more than 3 eV, corresponding to the $K\beta_1^h$ and $K\beta_3^h$ lines. In the first set the decay is due mainly to the $3p_{3/2}$ electron transition, whereas in the second set is mainly due to the $3p_{1/2}$ electron transition. LS coupling dominates the level structure for elements with $Z < 29$, as can be seen in Fig. 1 for Si. In this figure, the labels refer to the only transitions that contribute for the spectrum. Intercombination lines give negligible contribution.

3.2. Transition probabilities

The transition probability W^X for the line X is defined as

$$W^X = \frac{\sum_i N(i) W_i^X}{N(\gamma)} \quad (6)$$

where γ is, in this case, a given double-K hole configuration, $N(i)$ is a collection of excited atoms per unit volume and $N(\gamma) = \sum_i N(i)$. W_i^X is the transition probability for the line X from an initial level i , defined by

$$W_i^X = \sum_{f^X} W_{if}, \quad (7)$$

where f^X runs over all possible final levels in the radiative de-excitation process leading to the X line, and W_{if} is the probability per unit time that an atom in the excited level i , will decay to the level f , through the spontaneous emission of a photon.

For short lifetimes τ of the excited levels, compared with characteristic creating times (the inverse of the number of excitations per second undergone by one atom), the number of atoms doubly ionized in the K shell created in the excited level i per unit time $C_\gamma(i)$ equals the rate at which the atoms leave the level i , $N(i)/\tau(i)$, by all possible transitions. Assuming that the i level of a given double-K hole γ configuration is fed according their statistical weight, we have

$$C_\gamma(i) = C_\gamma \frac{g(i)}{g(\gamma)}, \quad (8)$$

where $g(i)$ and $g(\gamma)$ are the multiplicities of the i level and of the γ double-K hole configuration, respectively, and C_γ is the number of double-K ionised atoms created per unit time and per unit volume. From Eq. (6) and (8) we obtain

$$W^X = \frac{\sum_i g(i) \tau(i) W_i^X}{\sum_i g(i) \tau(i)}. \quad (9)$$

Using

$$\tau(i) = \frac{1}{\sum_f W_{if} + \sum_{f'} A_{if'}}, \quad (10)$$

where f runs for all possible final levels that can be reached by radiative transitions, with probabilities W_{if} , and f' runs for all possible final levels that can be reached by radiationless transitions, with probabilities $A_{if'}$, we get

$$W^X = \frac{\sum_i \frac{g(i)W_i^X}{W_i + A_i}}{\sum_i \frac{g(i)}{W_i + A_i}}. \quad (11)$$

We made use of $W_i = \sum_f W_{if}$, and $A_i = \sum_{f'} A_{if'}$.

For the elements where the two K-hole ground configuration has more than one level, it is therefore necessary to compute, for each of those levels, not only radiative transition probabilities, but also the radiationless (Auger) transition probabilities, to obtain the quantities W^X .

A complete calculation of radiative and radiationless decay rates from the double-K hole ground configuration was performed for Al and Sc. Radiative transitions include $K\alpha^h$ and $K\beta^h$ hypersatellite lines, as well as $K\alpha\alpha$ (one electron - two photon transitions) lines. The results are presented in Table 1 together with the total radiative and radiationless transition probabilities, for each of the two initial levels.

In Table 2 we provide the results of the complete calculation of W^X for the different lines in Al and Sc and of the statistical average transition probability of line X , defined as the quantity

$$W_{SA}^X = \frac{1}{g(\gamma)} \sum_i g(i) W_i^X \quad (12)$$

We observe that the values of W^X and W_{SA}^X are nearly identical. This results from the fact that Eq. (12) can be obtained from Eq. (11) if the summation $W_i + A_i$ has the same value for all initial levels. This is the case of Al and Sc presented in Table 1.

Total radiationless level widths are the sums of a large number of transition rates. We may assume that the relativistic effects tend to average out to some extent, similarly to what happens with total radiative widths [34]. To test this assumption, the value of radiationless (Auger) decay rate for each initial level of the Ti $2s^2 2p^6 3s^2 3p^6 3d^2 4s^2$ ground configuration was computed by adding the values of radiationless transition probabilities for all levels of the final $1s 2p^6 3s^2 3p^6 3d^2 4s^2$ configuration. As shown in Table 3, no significant variation of the decay rates was found for different initial levels, which shows that the radiationless decay rates do not depend significantly on the particular level of the initial configuration. This validates the use of Eq. (12) as a good value to W^X .

The ratio of the intensities of $K\beta_1^h$ to $K\beta_3^h$ hypersatellite lines computed in this work, with and without the Breit interaction, using the MCDF code of Desclaux and Indelicato, are presented in Table 4, together with the values obtained by Chen *et al*, which included Breit and vacuum-polarization corrections. We notice that our values for these ratios are larger than Chen's results for $Z \leq 40$. The two approaches yield ratios that are in good agreement for $Z > 40$.

In order to compare the transition energy values obtained in this work with experiment and calculations from other authors, we used the statistical average energy E_{SA}^X for the X line defined in our previous article [1] as

$$E_{SA}^X = \frac{1}{g(\gamma)} \sum_i g(i) \left(\frac{\sum_{f^X} E_{if} W_{if}}{\sum_{f^X} W_{if}} \right). \quad (13)$$

In this calculation we assumed that all i levels of the γ configuration are statistically populated. The quantity in parenthesis is the average energy of the X line, defined as the sum of the energies of all individual $i \rightarrow f$ transitions in the X line from an initial level i , E_{if} , weighted by the corresponding W_{if} radiative transition probability.

3.3. Widths of $1s^{-2}$ levels of Al and Sc

Using the values presented in Table 1, we were able to calculate the widths of the $1s^{-2}$ levels of Al and Sc, which are displayed in Table 5.

We believe this is the first time that level widths are calculated for a double-K hole level. These values can be compared with existing single-K hole level widths, using the expression $\Gamma(1s^{-2}) = 2\Gamma(1s^{-1})$.

For Al, using the Evaluated Atomic Data Library (EADL) value $\Gamma(1s^{-1}) = 0.37$ eV proposed by Campbell and Papp [35], we obtain $\Gamma(1s^{-2}) = 0.74$ eV, lower than the value calculated in this work. We note, however, that the experimental values of $\Gamma(1s^{-1})$ for Al referred to by the same authors are higher than their proposed value. Three of these values were derived from indirect measurements, using other level widths to obtain the $1s^{-1}$ level width. The only experiment that led directly to the $1s^{-1}$ level width yielded the value 0.47 eV.

For Sc, the same authors propose $\Gamma(1s^{-1}) = 0.83$ eV, which yields $\Gamma(1s^{-2}) = 1.66$ eV, in excellent agreement with the value obtained in this work.

3.4. Energy shifts

In Table 6 we present the results obtained in this work for the $K\beta_1^h$ and $K\beta_3^h$ energy shifts of the elements where we can distinguish these two lines.

This Table shows that our results for the $K\beta^h$ hypersatellites energy shifts, relative to the corresponding diagram line energies, are in good agreement with the results of Chen *et al* [10], ours being smaller by less than 0.2 % throughout.

To compare to the available experimental results, we present in Table 7 the $K\beta_{1,3}^h$ energy shifts calculated in this work. Our results agree in general with experiment, as it can be seen in Fig. 2, although the uncertainties of the latter are very large, with the exception of the recent experimental value of Diamant *et al* [7].

3.5. Breit interaction and QED corrections

To assess the contribution of the Breit interaction to the $K\beta^h$ hypersatellites energy shifts, we computed these shifts with and without inclusion of the Breit interaction in the calculation. We computed separately the $K\beta_1^h$ energy shifts, first with the Breit term (cf. Eq. (5)) included in the self-consistent process and the higher-order terms as a perturbation after the self-consistent process is finished, and then with Breit interaction neglected. The results are presented in Table 8. Although Chen *et al* [10] present their results for these shifts, obtained with the Dirac-Slater approach, in graphic form only, we easily conclude that our results, using the MCDF approach, are in very good agreement with the results of Chen *et al*.

The $K\beta_1^h$ to $K\beta_3^h$ intensity ratio is sensitive to the inclusion of the Breit interaction, similarly to Chen *et al* [10] finding for the $K\alpha_1^h$ to $K\alpha_2^h$ intensity ratio. The inclusion of this interaction decreases the $K\beta^h$ intensity ratio at low Z (21% for $Z = 18$) and increases it for medium and high Z ($\sim 5\%$ at $Z \simeq 50$). However, since relativity affects the $3p_{1/2}$ and $3p_{3/2}$ levels in a similar way the $K\beta^h$ intensity ratio increases monotonically towards the jj coupling limit of 2.

The evolution of the relative contribution of Breit interaction to the $K\beta_1^h/K\beta_3^h$ relative intensity ratio is illustrated in Fig. 3.

On the other hand, QED contributions for the energy shifts and transition probabilities have been found to be negligible. For instance, QED contributions for the $K\beta_1^h - K\beta_1$ energy shift in Hg is only 0.3% compared with 13% from the Breit interaction contribution, whereas for the $K\beta_1^h/K\beta_3^h$ intensity ratio the QED contribution is 0.05%, compared with 1.8% from the Breit contribution. The QED contributions for the $K\beta_1^h - K\beta_1$ energy shift are presented in Table 8.

4. Conclusion

In this work we used the MCDF program of Desclaux and Indelicato to compute energy shifts of the $K\beta_1^h$ and $K\beta_3^h$ hypersatellite lines relative to the parent diagram lines for several values of Z throughout the periodic table. One of the aims of this work was to assess the contribution of the Breit interaction to these shifts. Our results confirm the earlier findings of Chen *et al* [10] for these shifts and extended them to higher values of Z . We also calculated the $K\beta_1^h$ to $K\beta_3^h$ intensity ratio for the same values of Z . Our results are significantly lower than Chen *et al* values for the same ratios, for Z lower than 40, and agree with the values of these authors for higher values of Z . The total widths of the double-hole K levels of Al and Sc were also computed and our values were found in good agreement with the ones obtained from proposed values of single-K hole levels [35].

Acknowledgments

This research was partially supported by the FCT project POCTI/FAT/44279/2002 financed by the European Community Fund FEDER, and by the TMR Network Eurotraps Contract Number ERBFMRXCT970144. Laboratoire Kastler Brossel is Unité Mixte de Recherche du CNRS n° C8552.

References

- [1] Martins M C, Costa A M, Santos J P, Parente F and Indelicato P 2004 *J. Phys. B: At. Mol. Opt. Phys.* **37** 3785
- [2] Briand J P, Billy L, Charles P, Essabaa S, Briand P, Geller R, Desclaux J P, Bliman S and C. Ristori 1990 *Phys. Rev. Lett.* **65** 159
- [3] Moribayashi K, Sasaki A and Tajima T 1998 *Phys. Rev. A* **58** 2007
- [4] Briand J P, Chevallier P, Tavernier M and Rozet J P 1971 *Phys. Rev. Lett.* **27** 777
- [5] Briand J P, Chevallier P, Johnson A, Rozet J P, Tavernier M and A. Touati A 1974 *Phys. Lett. A* **49** 51
- [6] Briand J P, Touati A, Frilley M, Chevallier P, Johnson A, Rozet J P, Tavernier M, Shafroth S and Krause M O 1976 *J. Phys. B: At. Mol. Opt. Phys.* **9** 1055
- [7] Diamant R, Huotari S, Hämäläinen K, Sharon R, Kao C C and Deutsch 2003 *Phys. Rev. Lett.* **91** 193001
- [8] Deutsch M, Huotari S, Hamalainen K, Diamant R and Kao C -C 2000 *ESRF Annual Report 2000* Experiment number HE-790
- [9] Huotari S, Hämäläinen K, Diamant R, Sharon R, Kao C C and Deutsch 2004 *J. Electron. Spectrosc. Related Phenomena* **137** 293
- [10] Chen M H, Crasemann B and Mark H 1982 *Phys. Rev. A* **25** 391
- [11] Desclaux J P 1975 *Comp. Phys. Commun.* **9** 31
- [12] Indelicato P 1996 *Phys. Rev. Lett.* **77** 3323
- [13] Indelicato P and Desclaux J P, 2005 *MCDFGME, a MultiConfiguration Dirac Fock and General Matrix Elements program (release 2005)* <http://dirac.spectro.jussieu.fr/mcdf>
- [14] Indelicato P 1995 *Phys. Rev. A* **51** 1132
- [15] Ravenhall D E and Brow G E 1951 *Proc. R. Soc.* **208** 552
- [16] Sucher J 1980 *Phys. Rev. A* **22** 348
- [17] Mittleman M H 1981 *Phys. Rev. A* **24** 1167
- [18] Akhiezer A I and Berestetskii V B 1965 *Quantum Quantum Electrodynamics*
- [19] Lindgren I, Persson H, Salomonson S and Labzowsky L 1995 *Phys. Rev. A* **51** 1167
- [20] Mohr P J 1982 *Phys. Rev. A* **26** 2338
- [21] Mohr P J and Kim Y -K 1992 *Phys. Rev. A* **45** 2727
- [22] Mohr P J 1992 *Phys. Rev. A* **46** 4421
- [23] Indelicato P, Gorcex O and Desclaux J P 1987 *J. Phys. B: At. Mol. Opt. Phys.* **20** 651
- [24] Indelicato P and Desclaux J P 1990 *Phys. Rev. A* **42** 5139
- [25] Indelicato P, Boucard S and Lindroth E 1992 *Phys. Rev. A* **46** 2426
- [26] Indelicato P, Boucard S and Lindroth E 1998 *Eur. Phys. J. D* **3** 29
- [27] Indelicato P and Mohr P J 1991 *Theor. Chim. Acta* **80** 207
- [28] Blundell S A 1992 *Phys. Rev. A* **46** 3762
- [29] Blundell S A 1993 *Phys. Rev.* **T46** 144
- [30] Indelicato P and Mohr P J 2001 *Phys. Rev. A* **63** 052507
- [31] Boucard S and Indelicato P 2000 *Eur. Phys. J. D* **8** 59
- [32] Klarsfeld S 1969 *Phys. Lett.* **30A** 382

- [33] Fullerton L W and G. A. Rinker Jr G A 1976 *Phys. Rev. A* **13** 1283
- [34] B. Crasemann (ed) 1985 *Atomic Inner-Shell Physics* (New York, Plenum Press) p. 72
- [35] Campbell J L and Papp T 2001 *At. Data Nucl. Data Tables* **77** 1

Table 1. Radiative transition probabilities of $K\alpha\alpha$, $K\alpha^h$ and $K\beta^h$ lines, Auger and total transition probabilities for each initial level (LSJ_i) in Al ($Z = 13$) and Sc ($Z = 21$). Numbers in parenthesis indicate a power of ten.

		W_i^X (s^{-1})					W_i (s^{-1})	A_i (s^{-1})
	LSJ_i	$K\alpha_2^h$	$K\alpha_1^h$	$K\beta_{13}^h$	$K\alpha_2\alpha_3$	$K\alpha_1\alpha_3$		
Al	$^2P_{1/2}$	7.35(13)	6.74(11)	1.20(12)	9.37(10)	5.45(7)	7.55(13)	1.56(15)
	$^2P_{3/2}$	6.36(13)	5.40(11)	1.20(12)	1.00(11)	5.06(7)	6.55(13)	1.49(15)
Sc	$^2D_{3/2}$	4.93(14)	2.98(13)	7.04(13)	4.01(11)	1.69(9)	5.94(14)	1.91(15)
	$^2D_{5/2}$	4.88(14)	2.18(13)	7.01(13)	3.92(11)	1.19(9)	5.81(14)	1.95(15)

Table 2. Comparison between the results of a complete calculation W^X and a statistical average calculation W_{SA}^X of the transition probability for $K\alpha\alpha$, $K\alpha^h$ and $K\beta^h$ lines in Al ($Z = 13$) and Sc ($Z = 21$). Numbers in parenthesis indicate a power of ten.

		$K\alpha_2^h$	$K\alpha_1^h$	$K\beta_{13}^h$	$K\alpha_2\alpha_3$	$K\alpha_1\alpha_3$
Al	W^X (s^{-1})	6.68(13)	5.83(11)	1.20(12)	9.82(10)	5.19(7)
	W_{SA}^X (s^{-1})	6.69(13)	5.85(11)	1.20(12)	9.81(10)	5.19(7)
Sc	W^X (s^{-1})	3.96(14)	2.50(13)	7.02(13)	3.96(11)	1.39(9)
	W_{SA}^X (s^{-1})	3.96(14)	2.50(13)	7.02(13)	3.95(11)	1.39(9)

Table 3. Auger decay rates (ADR) per initial level (LSJ_i) of the Ti ground configuration $2s^2 2p^6 3s^2 3p^6 3d^2 4s^2$ obtained by adding the values of radiationless transition probabilities for all levels of the final configuration $1s 2p^6 3s^2 3p^6 3d^2 4s^2$.

LSJ_i	ADR (s^{-1})
3P_0	1.592(14)
1S_0	1.592(14)
3P_1	1.594(14)
3F_2	1.594(14)
1D_2	1.594(14)
3P_2	1.593(14)
3F_3	1.594(14)
3F_4	1.594(14)
1G_4	1.593(14)

Table 4. Ratio of the $K\beta_1^h$ to $K\beta_3^h$ hypersatellite lines intensities, $K\beta_1^h/K\beta_3^h$, computed in this work, with and without the Breit interaction included, and compared with Chen *et al* [10].

Z	$K\beta_1^h/K\beta_3^h$		
	This work		Chen
	Without Breit	With Breit	
18	0.020	0.017	0.0093
20	0.040	0.035	0.022
29	0.32	0.38	
30	0.44	0.45	0.389
36	0.84	0.88	0.831
38	0.96	1.00	
40			1.10
45			1.34
46	1.33	1.39	
47			1.42
48	1.39	1.46	
49			1.48
54	1.55	1.62	1.61
56	1.59	1.66	
60			1.72
65			1.75
70	1.77	1.82	
80	1.84	1.87	

Table 5. Values of widths for the $1s^{-2}$ levels of Al and Sc calculated in this work.

	LSJ_i	Γ_i (eV)
Al	$^2P_{1/2}$	1.079
	$^2P_{3/2}$	1.022
Sc	$^2D_{3/2}$	1.645
	$^2D_{5/2}$	1.669

Table 6. $K\beta_1^h$ and $K\beta_3^h$ energy shifts, in eV, computed in this work and compared with Chen *et al* [10].

Z	$E(K\beta_1^h)-E(K\beta_1)$		$E(K\beta_3^h)-E(K\beta_3)$		$E(K\beta_1^h)-E(K\beta_3^h)$
	This work	Chen	This work	Chen	This work
18	226.04	226.3	225.34	225.4	0.88
20	255.22	255.5	254.37	254.3	1.24
25		324.8		324.5	
29	381.62		381.14		2.96
30	396.03	397.4	396.52	397.0	3.43
31	412.10		412.15		3.65
36	491.47	492.3	491.22	492.1	8.25
38	524.43		524.17		10.87
40		558.8		558.6	
45		645.7		645.2	
46	662.45		661.86		28.67
47		681.8		681.2	
48	698.88		698.11		35.50
49	717.42	718.8	716.56	718.0	39.22
54	813.56	815.5	812.14	814.0	63.60
56	854.28		852.22		76.43
60		941.7		938.7	
65		1055.6		1051.1	
70	1175.10		1168.26		229.67
80	1451.49		1438.14		444.43

Table 7. The $K\beta_{1,3}^h$ energy shifts calculated in this work and the available experimental results.

Z	$K\beta_{1,3}^h - K\beta_{1,3}$ energy shifts (eV)	
	This work	Experiment
13	157.82	
14	171.34	
15	184.40	
16	197.63	
17	211.39	
18	225.24	
20	254.16	
21	267.66	
23	295.36	
25		345 ± 35^a
26	337.75	336.0 ± 0.5^b
27	351.85	
28	366.46	
29	380.36	
30	395.58	
31	411.01	390 ± 20^c
36	489.78	
38	522.60	
46	660.00	
48	696.26	
49	714.25	830 ± 60^c
54	810.42	
56	850.82	
70	1169.63	
80	1443.46	

^a Ref. [5]^b Ref. [7]^c Ref. [6]

Table 8. Breit and QED contributions to $K\beta_1^h$ energy shift.

Z	Breit		QED	
	(eV)	Percentage	(eV)	Percentage
18	1.66	0.7%	-0.08	-0.04%
20	2.31	0.9%	-0.10	-0.04%
29	8.59	2.0%	-0.30	-0.08%
30	8.30	2.1%	-0.29	-0.07%
36	14.77	3.0%	-0.47	-0.09%
38	17.50	3.3%	-0.54	-0.10%
46	31.96	4.8%	-0.88	-0.13%
48	36.54	5.2%	-0.99	-0.14%
54	52.79	6.5%	-1.61	-0.20%
56	59.51	7.0%	-1.53	-0.18%
70	121.72	10.4%	-2.96	-0.25%
80	188.49	13.0%	-4.59	-0.32%

Figure captions

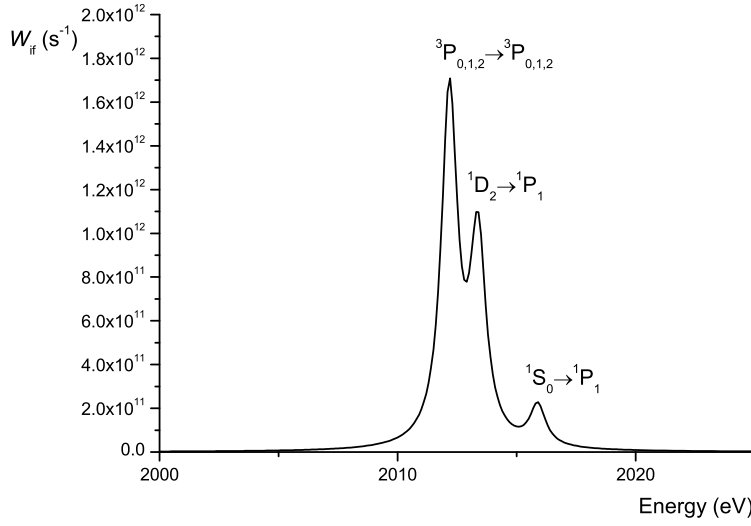


Figure 1. Calculated spectrum of Si $K\beta_{13}^h$ lines. A lorentzian with $\Gamma=0.8$ eV was used for each of the 14 transitions, which yield this profile.

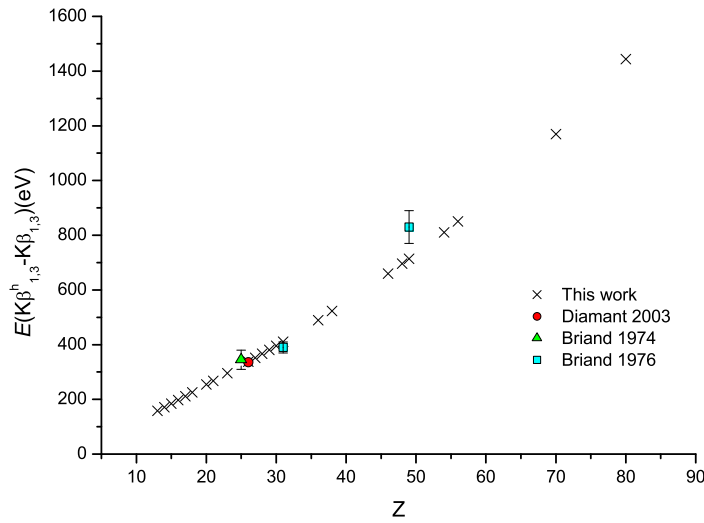


Figure 2. Calculated $K\beta_{1,3}^h$ energy shifts compared with available experimental results.

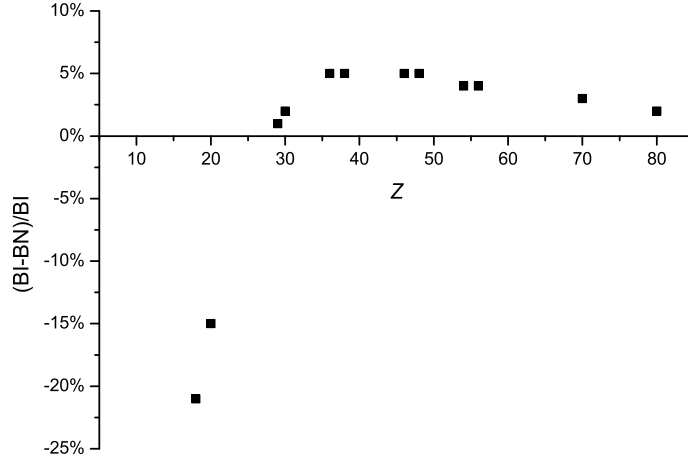


Figure 3. Relative contribution of Breit interaction on the $K\beta_1^h/K\beta_3^h$ intensity ratio. BI and BN stand for Breit included and Breit neglected, respectively.